The Egyptian Journal of Radiology and Nuclear Medicine (2011) **42**, 425–431

Egyptian Society of Radiology and Nuclear Medicine

The Egyptian Journal of Radiology and Nuclear Medicine

www.elsevier.com/locate/ejrnm
www.sciencedirect.com

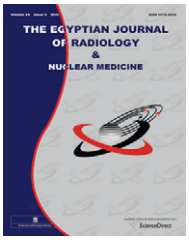

ORIGINAL ARTICLE

Influence of gamma emitter source intensity against energy on the image RMS contrast

R. Gholipour-Peyvandi *, S.Z. Islami-Rad, R. Heshmati, S. Zaferanlouie, M. Ghannadi-Maragheh

Nuclear Science and Technology Research Institute, AEOI, P.O. Box 14155-1339, Tehran, Iran

Received 4 July 2011; accepted 5 October 2011
Available online 4 November 2011

KEYWORDS

Intensity;
Energy;
Gamma source;
CT;
RMS contrast

Abstract Gamma energy and intensity are the key components in the reconstructed image, which play an important role in image quality of medical and industrial tomography equipments. In order to investigate and compare the effect of energy and intensity, a computed tomography (CT) system is designed and developed on the base of the first generation CT system. In this article we intended to compare the effect of intensity and energy on reconstructed image quality experimentally. To go through the process, several experiments are performed using ^{192}Ir (8 mCi), ^{75}Se (30 mCi) sources and mixture of ^{137}Cs (30 mCi)–^{75}Se (30 mCi) sources. Finally, the quality of different images is analyzed with RMS contrast to compare the effect of intensity and energy on image quality. The results show that energy and intensity have, respectively, inverse and direct relationship with RMS contrast of obtained images.

1. Introduction

Nuclear imaging systems, such as gamma computed tomography, are able to analyze and identify failures in industrial processes, permitting to visualize failure points (1,2). The goal of industrial gamma-ray CT is to produce internal images of object with sufficient detail to detect important features (3). The visibility of an image depends on the difference in gamma-ray attenuation between the features and its background (4).

Computed tomography is a noninvasive imaging technique that has been used extensively not only in medicine diagnosis and surgical planning, but also in nondestructive testing (NDT) for many industrial applications such as mechanical part manufacturing, production of composite materials, waste

* Corresponding author. Tel.: +98 021 82062572.
E-mail addresses: rgholipour61@yahoo.com (R. Gholipour-Peyvandi), szislami@yahoo.com (S.Z. Islami-Rad).

0378-603X
Peer review under responsibility of Egyptian Society of Radiology and Nuclear Medicine.
doi:10.1016/j.ejrnm.2011.10.003

Production and hosting by Elsevier

container inspection, metrology, detection of structural defects and others, heterogeneities in polymer objects, etc. (5–8).

Contrast is usually used to assess the performance of a gamma-ray CT (3). In gamma-ray CT, the contrast is affected by several factors. These factors are detector, collimator, counting time, etc. Gholipour et al. studied the effect of beam width on reconstructed image contrast. Their results demonstrated that for a constant source collimator aperture, the RMS contrast increases as the detector collimator aperture increases. Also, for a constant detector collimator aperture, the RMS contrast increases as the source collimator apertures increases even though the variation is negligible. The acquired results of beam width can be performed on industrial and medical gamma-ray CT to improve reconstructed image contrast and reduce absorbed dose and radiation exposure in patients and optimize the results of gamma-ray CT (9). Wu and Liu have reported experimental research on rear collimator in gamma-ray industrial CT, which plays an important role in suppressing scattered radiation and improving the CT performance (4). Gholipour et al. and Vasquez et al. have investigated the influence of gamma energy on the image contrast for material with different density and counting time and shown that contrast is better in lower energy and higher counting time. Furthermore, the quality of constructed images can be improved by using extensive range of density (10–11). De Mesquita et al. developed industrial CT with a plastic scintillator position sensitive detector using Monte Carlo method and simulated the effect of geometry which the results are valid experimentally (12).

In this article, we would like to illustrate energy and intensity factors that mainly influence in the contrast. Firstly, the basic theory is defined, and then test setup and experiment condition are explained. Finally, the test outcome is comprehensively discussed and compared with previous works.

2. Theory

Here, we investigate the effects of energy and intensity on quality of industrial CT images. Tomography imaging consists of directing γ-rays into an object from multiple orientations and measuring intensity decrease along a series of linear paths. The intensity reduction is characterized by Beer's law which describes it as a function of γ-ray energy, path length, and linear attenuation coefficient of material. Finally, a specialized algorithm is used to reconstruct the images (13).

A special data acquisition software is designed that enables multi-energy window to be produced at each projection. This method helps to compare the effects of energy and intensity of a spectrum. The sources in this experiment are ^{192}Ir, ^{75}Se and mix source ^{137}Cs–^{75}Se which energy and intensity of their spectrum are theoretically and experimentally illustrated in Fig. 1.

2.1. Radon transform

The Radon transform computes projections of an image. The Radon transform can be defined as the collection of projections of an object gathered at various angles. In a gamma-ray transmission, I, of a mono-energetic radiation beam traversing a phantom of thickness is given by the following equation:

$$g = Ln(I_0/I) = \int_L \mu(x,y)du \tag{1}$$

where I_0 is the incident beam intensity of the radiation beam, du is some different path length, $\mu(x, y)$ is the function describing the two dimensional distribution of attenuation coefficient in the imaged object at the point (x, y), g, the transmittance of the object, is defined as the logarithm of the ratio of the intensity of the detected beam to the intensity of the emitted beam and L is the line along which the beam travels. The line L can be represented uniquely by the parameters r and θ, where θ measures the counterclockwise angle of the line from the vertical, and r measures the distance of the line from the origin of the (x, y) plane. Thus, we can use the above formula to define a transform which maps a function $f(x,y)$ to a function $g(r, \theta)$, where $g(r, \theta)$ is the line integral of $f(x,y)$ over the line defined by r and θ. This transform is known as the Radon transform and denoted by R which the Radon transform of $f(x, y)$ at same angle θ is the line integral of f parallel to the y axis:

$$R_\theta(x') = \int_{-\infty}^{+\infty} f(x'\cos\theta - y'\sin\theta, x'\sin\theta + y'\cos\theta)dy' \tag{2}$$

$$\begin{bmatrix} x' \\ y \end{bmatrix} = \begin{bmatrix} \cos\theta & \sin\theta \\ -\sin\theta & \cos\theta \end{bmatrix} \begin{bmatrix} x \\ y \end{bmatrix} \tag{3}$$

The function $R_\theta(x')$ is often referred to as a sinogram because the Radon transform of an off-center point source is a sinusoid. The task of tomographic reconstruction is to find $\mu(x, y)$ given knowledge of $R_\theta(x')$, therefore the Filter Back Projection algorithm is used to reconstruct from the measured projections by the filtered back projection method to bring about the inverse Radon transformation. The FBP algorithm begins by filtering the Radon transform data. There are many filters which can be used in our experiments; we used the Ram–Lak filter to remove some of the high-frequency components that are often fraught with noise. Geometrically, the back projection operation simply propagates the measured sinogram back into the image space along the projection paths (14–16).

2.2. RMS contrast

The RMS contrast in each image demonstrates the effect of following factors on image quality. In the reconstructed image, contrast is a criterion which shows the color diversity of images and the difference in visual properties that makes an object (or its representation in an image) distinguishable from other objects and the background. There are some definites for calculating contrast. In this paper, RMS contrast was selected to compare image qualities. RMS contrast does not depend on the spatial frequency content or the spatial distribution of contrast in the image. RMS contrast is defined as the standard deviation of the pixel intensities.

$$\text{RMS contrast} = \sqrt{\frac{1}{MN}\sum_{i=0}^{N-1}\sum_{j=0}^{M-1}(I_{ij} - \bar{I})^2} \tag{4}$$

where intensities I_{ij} are the i-th and j-th elements of the two dimensional image of size $M \times N$. $\bar{I}$ is the average intensity of all pixel values in the image. The pixels of image I are normalized to have intensity value in the range of (0, 1). In order to compare all reconstructed images, energy windows are normalized to intensity rang that have most value, in the other words (0,1) for normalization are related to one window

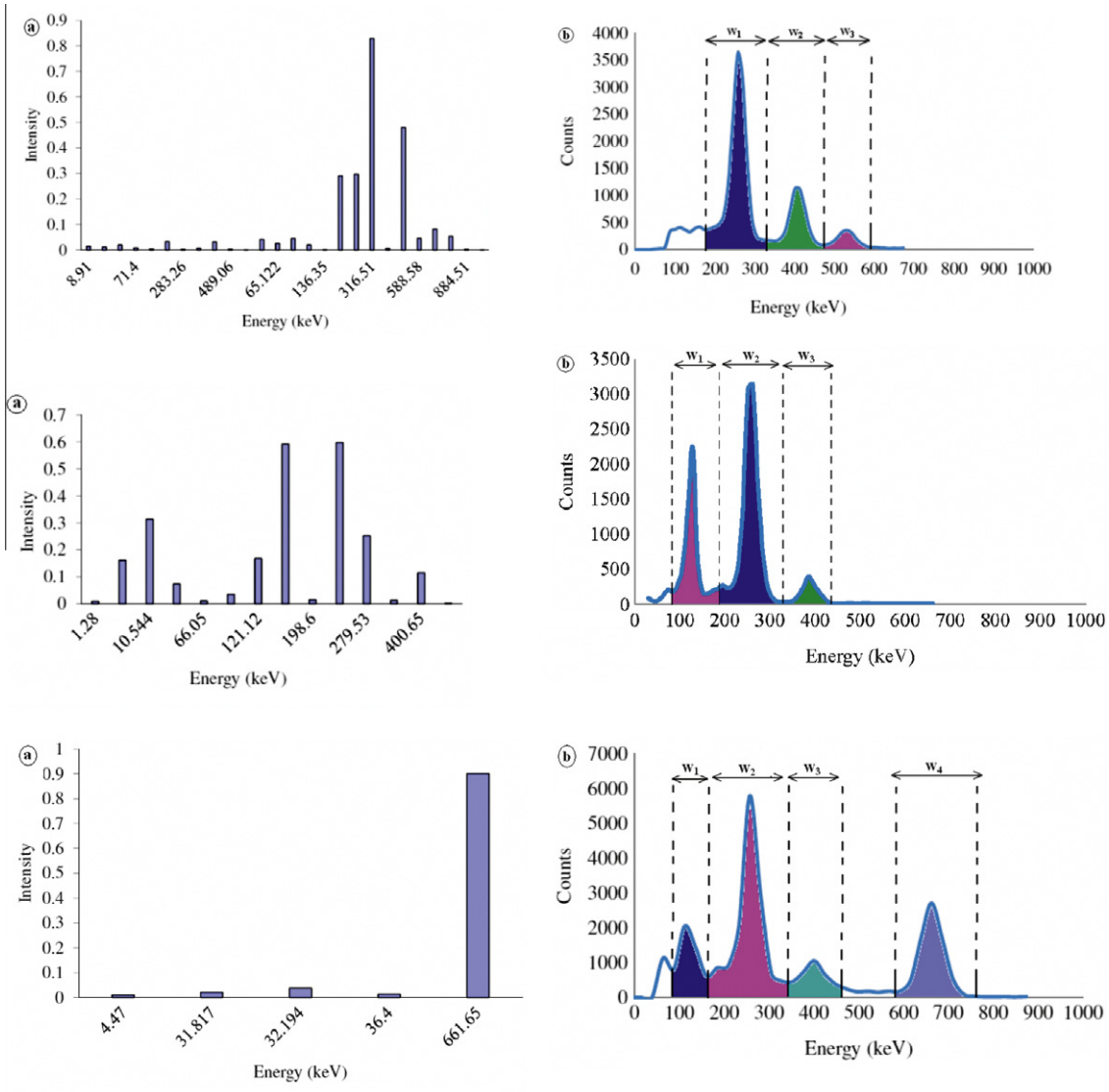

Figure 1 The energy and intensity spectrum (a) for applied sources (^{192}Ir, ^{75}Se and ^{137}Cs) as theory (b) for applied sources (^{192}Ir, ^{75}Se and ^{137}Cs–^{75}Se) as experiment using NaI(Tl) (2×2, 905-3 model, Eberline company with 6% resolution for ^{137}Cs).

which it has most variety in color spectrum. It is particularly necessary to note that these experiments were performed in the same condition and are repeatable. As a result, image noise and artifacts can not affect RMS contrast (17,18).

3. Experimental setup

A single-source – single-detector gamma computed tomography (CT) scanner system was used in this study. In this setup, a NaI(Tl) detector 5.08 cm in diameter is located opposite the center of the source in distance 55 cm, and applied sources are ^{192}Ir (8 mCi), ^{75}Se (30 mCi) and mix source ^{137}Cs (30 mCi)–^{75}Se (30 mCi). The detector and the source are aligned by a point semiconductor laser; also two cylindrical lead collimators (5 mm diameter) were used for source and detector (Fig. 2). The position of phantom is defined by three motors, which a schematic design of the system hardware is shown in Fig. 3. The phantom rotated by step 5° ($\Delta\theta = 5°$) and moved in the direction of r with $\Delta r = 1.5$ mm. The CT scans are taken out by scanning 180° to collect attenuation beams. There are 85×35 ($r \times \theta$) projections for producing of image and time of each projection is selected to be 3 s. A polyethylene phantom (0.93 g·cm^{-3}) is used to determine the two dimensional imaging quality of the designed industrial CT system. The phantom is made as cylindrical geometry on which three holes of 15 mm in diameter are improvised. The holes are filled with mercury (13.53 g·cm^{-3}), iron (7.874 g·cm^{-3}) and air (1.184 mg·cm^{-3}). Nuclear electronic system consists of a NaI(Tl) (2×2, 905-3 model, Eberline company with 6% resolution for ^{137}Cs), and a specialized MCA (PSS-1, NSTRI, Tehran, Iran) that consists of a pre-amplifier, amplifier, high voltage (HV) and data acquisition system. In this MCA, universal written software can simultaneously read positions and steps, control the motors and MCA. After that, the image is reconstructed from the

Figure 2 Configuration of source and detector collimator.

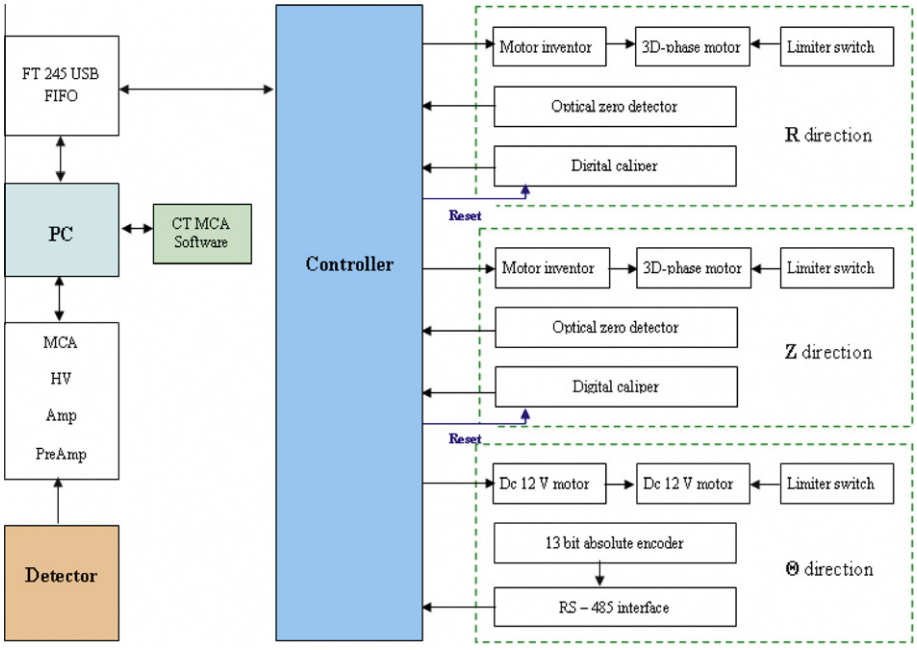

Figure 3 Computed tomography system hardware diagram.

measured projections by the filtered back projection method to bring about the inverse Radon transformation. The produced image is due to about 3000 projections.

4. Results and discussion

The behavior of energy and intensity effects is measured with ^{192}Ir, ^{75}Se, ^{137}Cs–^{75}Se sources and the phantom with three holes. The results that we report here are RMS contrast of reconstructed images. Thus, the produced images with different widths of energy and variety relative intensity are tested in different study cases. The first case (a–c) represents the results with a source of ^{192}Ir (8 mCi), a collimator (5 mm diameter), a phantom with three holes and the energy widths of 190–371 keV, 371–525 keV, 525–665 keV and relative intensity of 100%, 31%, 8.9%, respectively. The second case (d–f) represents the results with a source of ^{75}Se (30 mCi), the energy widths of 84–190 keV, 190–370 keV, 370–453 keV and relative intensity of 61.5%, 100%, 9.25%, respectively. The third case (g–j) represents the results with a mix source of ^{137}Cs–^{75}Se, with the energy widths of 88–160 keV, 160–331 keV, 331–487 keV, 574–784 keV and relative intensity of 35.9%, 100%, 17.2%, 45.6%, respectively (Fig. 4).

A listing of the RMS contrast components for each image with different energy and relative intensity spectrum are shown in Table 1.

According to Fig. 4 and Table 1, the best RMS contrast for ^{192}Ir is obtained in the first window with low energy and high intensity. By increasing energy and reducing intensity, RMS contrast decreases in the succeeding windows when these results are predictable according to previous papers. ^{75}Se source, has less energy and intensity in the first window than in the second one when its results represent better RMS contrast for the second window. Acquired results from ^{192}Ir and ^{75}Se sources are also confirmed by the mix source of ^{137}Cs–^{75}Se which they show the image of second window have the best RMS contrast compared with third and forth window. Moreover, in the forth window with more energy and intensity than the first and third window, we have better RMS contrast. Thus two factors, energy and intensity have a strong effect on contrast improvement of images.

5. Conclusion

The experimental measurements show the effect of energy and intensity on reconstructed image quality. The RMS contrast increases as energy factor decreases, although the

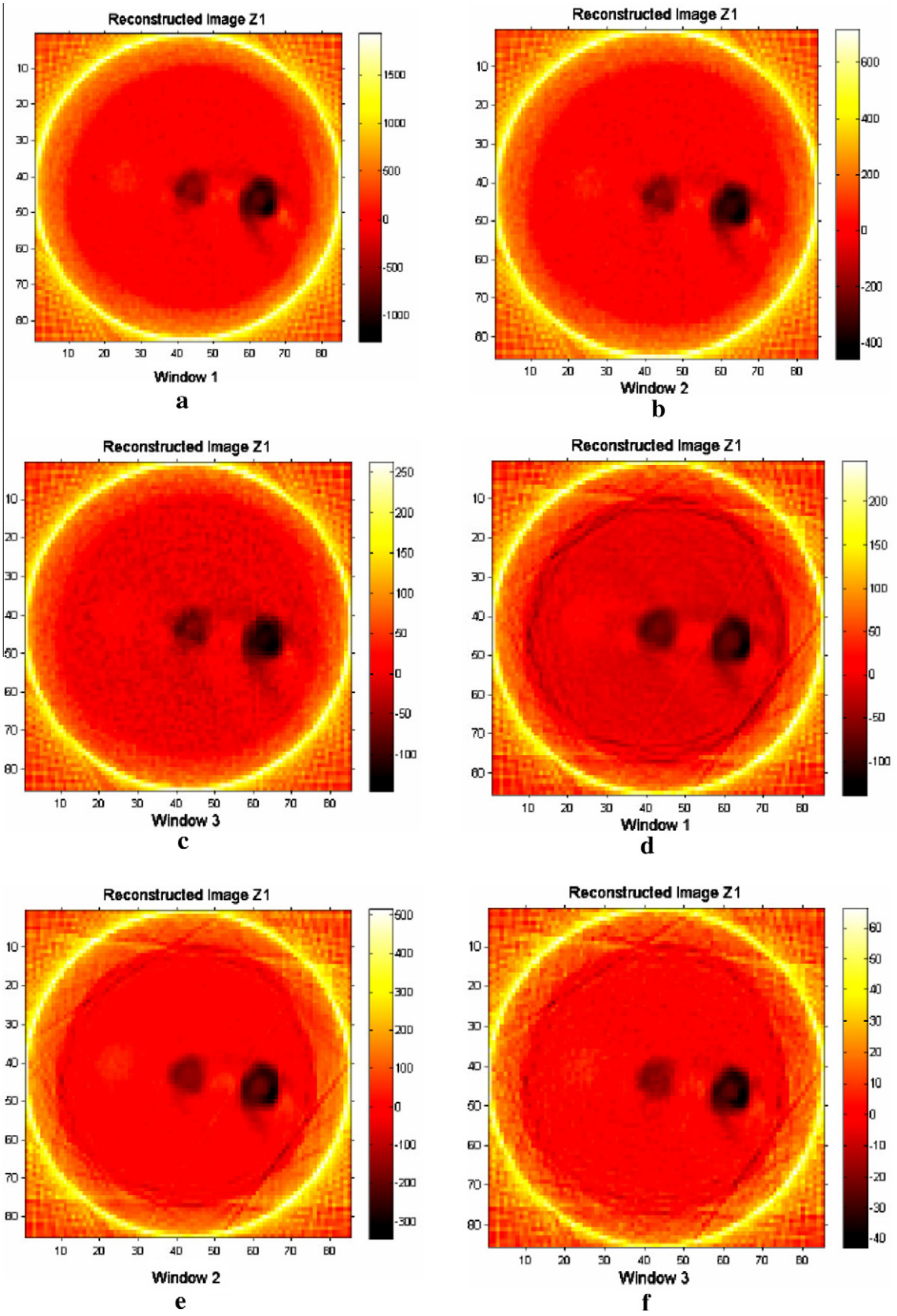

Figure 4 Polyethylene phantom two dimensional image, mercury, iron, air holes with different energy and intensity: (a–c) ^{192}Ir source; (d–f) ^{75}Se source, 75; (g–j) ^{137}Cs–^{75}Se source.

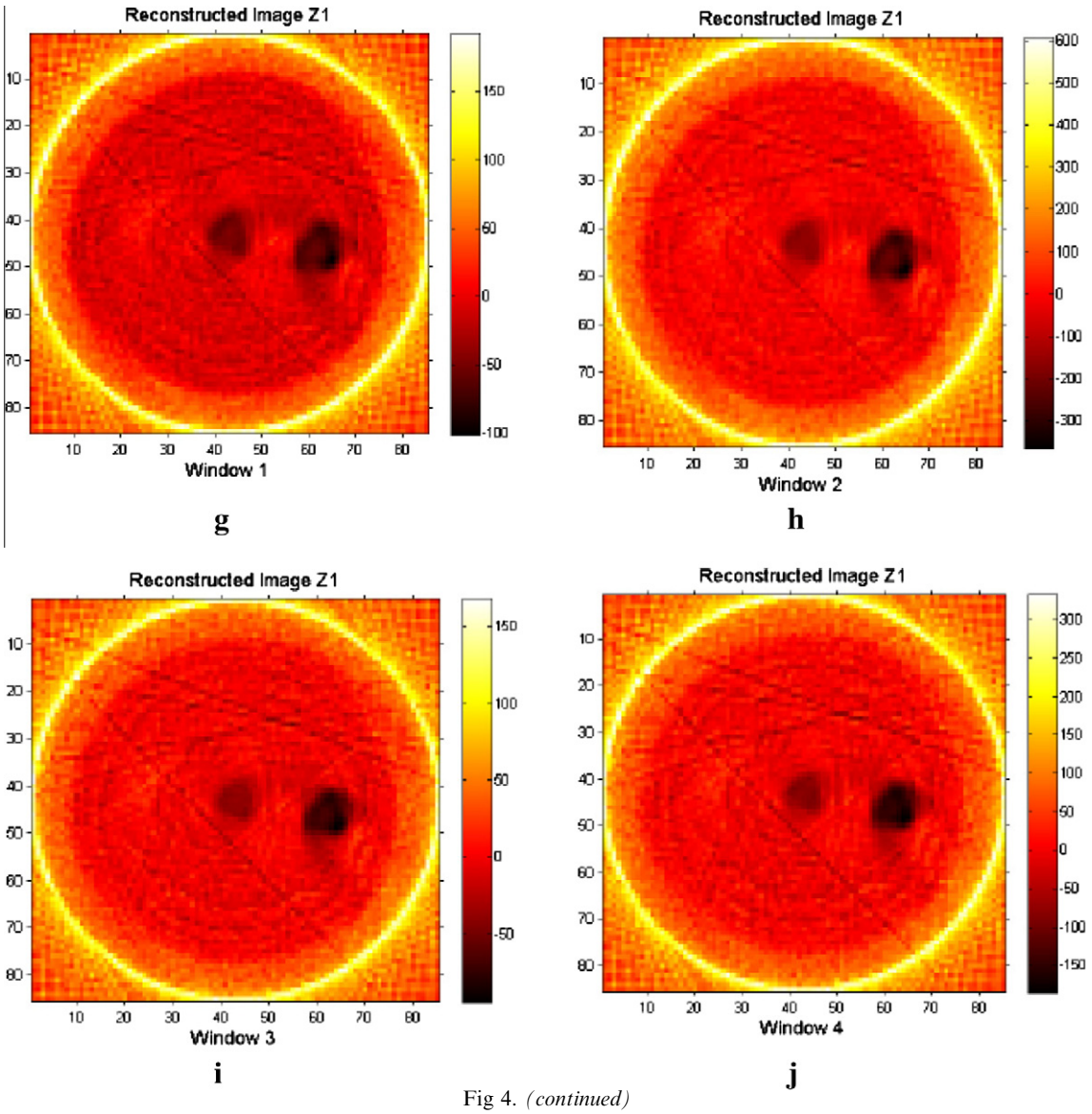

Fig 4. *(continued)*

Table 1 RMS contrast for comparing different energy and intensity effects.

Source	Energy (keV)	Relative intensity (%)	RMS contrast ($\times 10^{-4}$)	Fig. 4
^{192}Ir	190–371	100	551	(a)
	371–525	31	210	(b)
	525–665	8.9	69	(c)
^{75}Se	84–190	61.5	203	(d)
	190–370	100	524	(e)
	370–453	9.25	72	(f)
Mix source (^{137}Cs–^{75}Se)	88–160	35.9	156	(g)
	160–331	100	542	(h)
	331–487	17.2	155	(i)
	574–784	45.6	321	(j)

intensity factor has direct relationship with RMS contrast. Also, the results represent that for energy factor and relative intensity applied in experiment, the effect of relative intensity factor on RMS contrast is more than energy factor.

In the medical and industrial tomography the accuracy of images has direct relationship with intensity and increasing this factor improves quality of the image. Therefore, two factors of energy and intensity should be optimized to obtain an appropriate tomography.

References

(1) Noel J. Advantages of CT in 3D scanning of industrial parts, vol. 1. Scanning Technologies Magazine, 2008; 18.

(2) De Oliveira Jr JM, Martins ACG, de Milito JA. Analysis of concrete material through gamma ray computerized tomography. Braz J Phys 2004;34:1020–3.

(3) IAEA-TECDOC 1589. Industrial process gamma tomography. Final report of a coordinated research project 2003–2007. Austria: International Atomic Energy Agency; 2008.

(4) Wu ZH, Liu J. Experimental research on rear collimator in γ-ray industrial CT. Appl Radiat Isot 2009;67:1216.

(5) Calvo WAP, Hamada MM, Sprenger FE, Vasquez PAS, Rela PR, Martins JFT, et al.. Gamma-ray computed tomography SCANNERS for applications in multiphase system columns. Nukleonika 2009;54:129.

(6) Camp DC, Martz HE, Roberson GP, Decman DJ, Bernardi RT. Nondestructive waste-drum assay for transuranic content by gamma-ray active and passive computed tomography. Nucl Instrum Methods A 2002;495:69–83.

(7) Lettenbauer H, Georgi B, Weiß D. Means to verify the accuracy of CT systems for metrology applications (in the absence of established international standards). In: DIR 2007 – international symposium on digital industrial radiology and computed tomography, Lyon, France, 2007.

(8) Braz D, Lopes RT, Da Motta LMG. Computed tomography: an evaluation of the effect of adding polymer SBS to asphaltic mixtures used in paving. Appl Radiat Isot 2000;53:725–9.

(9) Gholipour Peyvandi R, Islami Rad SZ, Ghannadi Maragheh M. Study of beam width on reconstructed image contrast using the first generation gamma ray. Instrum Exp Tech 2011;54:149–53.

(10) Gholipour Peyvandi R, Islami Rad SZ, Ghannadi Maragheh M. Int J Pure Appl Phys 2010;6:447–56.

(11) Vasquez PAS, de Mesquita CH, Hamada MM. Phantom study using a first generation gamma tomography system. In: International nuclear atlantic conference – INAC 2007, Brazil, Santos, 2007.

(12) De Mesquita CH, Legoupil S, Hamada MM. Development of an industrial computed tomography designed with a plastic scintillator position sensitive detector. In: IEE nuclear science symposium conference record, Fajardo, Puerto Rico, 2005:540–4.

(13) Kim J, Jung S, Kim J. A study on industrial gamma ray CT with a single source–detector pair. Nucl Eng Tech 2006;38:383–9.

(14) Herman GT. Fundamentals of computerized tomography: image reconstruction from projections. 2nd ed. USA: Springer; 2009.

(15) Bushberg JT, Seibert A, Leidholdt EM, Boone JM. The essential physics of medical imaging. 2nd ed. Philadelphia, USA: Lippincott Williams & Wilkins; 2000.

(16) Deans SR. The radon transform and some of its applications. New York, USA: John Wiley & Sons; 1983.

(17) Herman GT. Image reconstruction from projections. 1st ed. London, England: Academic Press; 1980.

(18) Peli E. Contrast in complex images. J Opt Soc Am 1990;7:2032–40.